Chemical Engineering Journal 246 (2014) 287–298

Contents lists available at ScienceDirect

Chemical Engineering Journal

journal homepage: www.elsevier.com/locate/cej

Ceramic papers as flexible structures for the development of novel diesel soot combustion catalysts

F.E. Tuler [a], E.D. Banús [a], M.A. Zanuttini [b], E.E. Miró [a], V.G. Milt [a,*]

[a] Instituto de Investigaciones en Catálisis y Petroquímica, INCAPE (FIQ, UNL – CONICET), Santiago del Estero 2829, 3000 Santa Fe, Argentina
[b] Instituto de Tecnología Celulósica, ITC (FIQ, UNL), Santiago del Estero 2654, 3000 Santa Fe, Argentina

HIGHLIGHTS

- Flexible ceramic papers were prepared for diesel soot abatement.
- Cobalt and cerium oxides were impregnated to develop catalytic activity.
- Cerium nanoparticles, added to confer mechanical resistance, allowed anchoring catalytic species.
- A filter designed from catalytic papers properly resisted testing bench experiments.

GRAPHICAL ABSTRACT

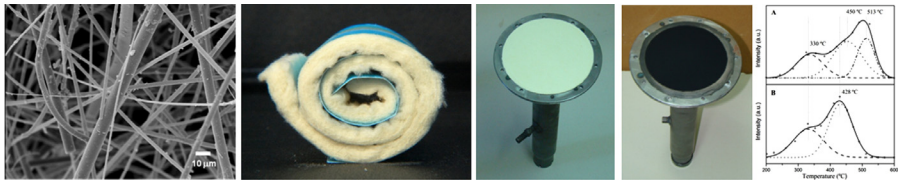

Catalytic ceramic paper with an open structure. | Flexible developed ceramic papers. | Soot filter based on a ceramic paper before and after a testing bench experiment. TPO curves.

ARTICLE INFO

Article history:
Received 9 December 2013
Received in revised form 5 February 2014
Accepted 25 February 2014
Available online 12 March 2014

Keywords:
Diesel filters
Ceramic papers
Structured catalysts
Soot removal
Co–Ce catalysts

ABSTRACT

Currently, the most adequate technology for the abatement of particles coming from diesel engines is the one that employs catalytic filters. This work proposes the preparation of catalytic ceramic papers to be employed in the development of new catalytic filters. To this end, the papermaking technique was employed. The resulting papers were flexible, easy to handle and presented suitable mechanical properties to resist the tests from a test bench in which they were placed inside a metal housing, at the exhaust pipe outlet of a Corsa 1.7 vehicle. These optimal mechanical properties were obtained through the incorporation of a suspension of CeO_2 nanoparticles during the papermaking process. It was found that the nanoparticles covered the ceramic fibers completely and that their excess accumulated under the form of patches. In order to promote the filter continuous regeneration, once the ceramic papers were formed they were impregnated with a cobalt salt which, after a calcination stage, produced oxidic clusters in tight contact with the CeO_2 nanoparticles. The papers thus obtained exhibited a maximum soot combustion temperature close to 400 °C, being T_{50} = 376 °C for the more active catalytic ceramic paper, in the presence of NO (1000 ppm) in the feed. Even though more tests are necessary to determine filtration efficiency, preliminary experiments carried out in the test bench proved that the ceramic papers properly resisted the high gas flow rates of fumes emitted by a real diesel engine (approximately 2 m^3 min^{-1}). From the TPO experiments performed on samples of catalytic ceramic papers taken from the test bench and in tight contact with the soot retained, it was possible to obtain a maximum soot combustion temperature equal to 428 °C. It was also found that the presence of ceria aggregates caused the papers to deactivate to a lesser degree after being treated at 900 °C.

* Corresponding author.
E-mail addresses: vmilt@fiq.unl.edu.ar, vivimilt@live.com.ar (V.G. Milt).

http://dx.doi.org/10.1016/j.cej.2014.02.083
1385-8947/

1. Introduction

Diesel engines are widely employed both in light and heavy vehicles due to their durability, reliability and fuel economy. Today, 60% of the vehicles sold in Europe are driven by diesel engines and they are also extensively used all over the world. However, the exhaust gases emitted by these engines have very high concentrations of particulate material (soot) and nitrogen oxides, which are harmful to human health [1,2].

Both particulate matter and nitrogen oxides are also harmful to the environment, acid rain and photochemical smog being among the adverse effects they provoke. For this reason, the legislation related to polluting emission control includes increasingly stricter standards. Standard Euro 6, which is to be implemented in 2014, maintains the values of particulate matter emitted by light vehicles up to 0.0045 g/km and the maximum number of particles emitted per km to 6.10^{11} but reduces the amount of nitrogen oxides (from 0.18 to 0.08 g NOx/km) [3].

The values mentioned above imposed by the EU directives cannot be achieved only by modifying the engines or by adding promoters to the fuel. Post-combustion treatments of exhaust fumes are also mandatory. So far, the most adequate treatment to abate particulate matter consists in employing filters capable of retaining the soot particles. These filters should be chemically, thermally and mechanically resistant to adequately endure the operating conditions, especially during the regeneration step that could originate high temperature peaks [4]. Besides, they should have a good filtering capacity to efficiently retain the soot particles present in the exhaust gases from diesel engines [5].

Different types of structures have been considered for the development of filters, monoliths and foams being the most widely studied ones [6–8]. Today's commercial filters are flow-through type SiC monoliths. As an attractive alternative, the use of flexible substrates would allow the filtering element to adapt to any geometry or shell, providing a more versatile filter. The paper-type structure, composed of a network of fibers interconnected through pore-type spaces provides a beneficial reaction environment which favors the gas diffusion through the catalytic bed [9]. Employing ceramic and cellulosic fibers during paper preparation produces ceramic papers resistant to severe thermal conditions after calcination (temperatures above 900–1000 °C).

In this context, the aim of this work is to employ the above described structures to develop filters for the treatment of diesel engine exhaust gases. The addition of catalysts to these structures allows obtaining catalytic filters with which self-regenerating systems could be obtained. Different catalysts have proved to be active in the temperature range of diesel engines exhaust gases, which varies upon speed, type of motion and the vehicle itself. However, at present, it is possible to heat the exhaust gases slightly without implying a significant demand of energy. Therefore, active catalysts at temperatures slightly above 350 °C can be considered suitable to be incorporated to the filters in order to achieve their continuous regeneration.

In a previous work, we studied the addition of KNO_3 to ceramic papers [10] and found that the catalytic activity of this system was acceptable (maximum soot combustion temperature = 395 °C). But, even though the addition of potassium improves the soot-catalyst contact and allows obtaining catalytically active systems, its volatility is high and therefore its use is not advisable.

Cobalt and cerium oxides were selected as active materials for filter regeneration. Studies of the Co_3O_4–CeO_2 mixed system [11–13] for soot combustion report a maximum combustion rate temperature of 500 °C for mixtures Co_3O_4 (20% molar) – CeO_2, working with a soot/catalyst ratio = 1/20, soot/catalyst mixtures with loose contact and an oxygen concentration in the feed stream of 15% [12]. In this vein, Banús et al. [14] studied the behavior of Co_3O_4–CeO_2 catalysts supported on metallic foams. The combustion activity of these structured catalysts was higher than the one corresponding to the powder catalysts for soot/catalyst mixtures in loose contact and slightly lower than that of the powder catalysts in tight contact.

In this work, CeO_2 nanoparticles were added during the preparation of ceramic papers in order to improve their mechanical properties. Cobalt was added as active component by impregnation of the ceramic paper disks with a cobalt nitrate solution. The systems thus developed were tested for the diesel soot combustion through TPO experiments carried out under laboratory conditions. Besides, in order to collect real soot particles, the catalytic ceramic papers were introduced into a metallic housing and tested in test bench with a Corsa 1.7 diesel engine.

2. Experimental

2.1. Ceramic paper preparation

The preparation method of the ceramic paper was based on a procedure similar to that used in the production of conventional paper from cellulose fibers. The ceramic fibers (50 wt.% SiO_2, 48 wt.% Al_2O_3, 2 wt.% impurities), obtained from CARBO ceramic material by elutriation, were dispersed in the aqueous medium in which a binder was added (commercial nanoparticles of CeO_2, NYACOL) to give mechanical resistance to the final ceramic paper. Cellulose fibers were also needed in order to properly form the paper matrix because they have an average length of about 3000 μm and are longer than the ceramic ones, of about 660 μm in length. Their length and ribbon shape helped retain the ceramic fibers during the formation stage. They were obtained by repulping an industrial blotting paper produced from virgin softwood Kraft slightly-refined fibers. The method required the addition of both cationic and anionic polyelectrolytes in order to form a double layer over the ceramic fibers and catalytic particles so as to favor the formation of the catalytic paper structure. The cationic polymer used was polyvinyl amine (PVAm) (Luredur PR 8095) from BASF and the anionic polymer was anionic polyacrylamide (A-PAM) from AQUATEC.

A two-step method was employed for the preparation of catalytic ceramic papers. In the first step, 1000 ml NaCl solution 0.01 N were stirred into a vessel. Several ingredients were incorporated every 3 min under constant moderate stirring (66 ml of cationic polyelectrolyte, 10 g of ceramic fibers, the CeO_2 colloidal suspension in different percentages with respect to the amount of ceramic fiber – 10 or 20 wt./wt.% as CeO_2 – 42 ml of anionic polyelectrolyte and, finally, 1.5 g of cellulosic fiber). With this suspension, a sheet was structured using the SCAN standard method (SCAN-C 26:76 and SCAN-M 5:76), applying a pressing pressure greater than the one established by the above mentioned standards for the preparation of cellulosic papers (37.5 kPa). The sheet (16.5 cm in diameter) was dried under controlled atmosphere (23 °C, 50%RH) for 24 h and finally calcined in air at 600 °C for 2 h.

The second step corresponded to the incorporation of the catalytic ingredients by impregnation of the ceramic paper discs with solutions of $Ce(NO_3)_3$ and $Co(NO_3)_2$, both with a 0.25 M concentration. Although Ce was already present as a binder, we found that the addition of the Ce salt was beneficial to improve the catalytic activity. The total amount of cerium coming from both the CeO_2 Nyacol suspension and the $Ce(NO_3)_3$ solution was intended to be kept constant in ca. 30 wt.% of atomic cerium. The calcined paper was uniformly impregnated by dripping a solution with the desired component and then calcined again at 600 °C for 2 h. In the case of papers containing both cobalt and cerium, each one

of these elements was separately incorporated by impregnation, first Ce and then Co, as previously described, with an intermediate calcination step after each impregnation. Cerium and cobalt were separately incorporated, cobalt in a second step, so as to keep as much as possible of the transition metal on top of the ceramic fibers.

Fig. 1 shows a diagram with the synthesis sequence of the different papers prepared. Table 1 summarizes the nomenclature adopted to denote the different ceramic papers prepared, as well as the cerium and cobalt content of each paper.

In order to study the thermal stability of the catalytic ceramic papers, some of them were treated at 900 °C during 2 h.

2.2. Characterization

2.2.1. X-ray diffraction (XRD)

Crystalline phases were determined with a Shimadzu XD-D1 instrument with monochromator using Cu Kα radiation at a scan rate of 1 °/min, from $2\theta = 25°$ to 80°. The pieces of about 2 cm × 2 cm were supported in a special sample holder designed for the XRD analysis. The software package of the equipment was used for the phase identification from the X-ray diffractograms.

2.2.2. Laser Raman spectroscopy (LRS)

A Horiba JOBIN YVON LabRAM HR instrument was used to obtain the spectra. The excitation source was the 514.5 nm line of a Spectra 9000 Photometrics Ar ion laser with the laser power set at 30 mW. Several spectra were acquired for each sample.

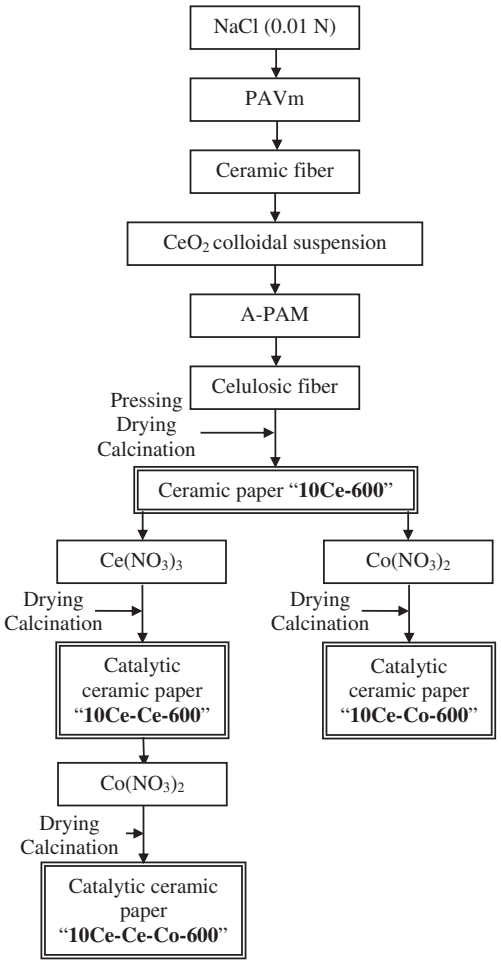

Fig. 1. Synthesis of the catalytic ceramic paper. Stages of the preparation procedure (example for papers with 10 wt.% CeO_2 and calcined at 600 °C).

2.2.3. Scanning Electron Microscopy (SEM) and Energy Dispersive X-ray Spectroscopy (EDX)

A SEM Jeol JSM-35C equipment was employed operated at 20 kV acceleration voltage. Samples were glued to the sample holder with Ag painting and then coated with a thin layer of Au in order to improve the images.

The elemental chemical analysis was performed trying the EDX spectra with the EDAX software. Semi quantitative results were obtained with the theoretical quantitative method (SEMIQ), which does not require standards. EDX spectra were obtained with an acceleration of 20 kV.

2.2.4. Temperature-programmed oxidation (TPO)

2.2.4.1. Experiments with soot obtained from burning diesel fuel. Soot particles were produced by burning a commercial diesel fuel (YPF, Argentina) in a glass vessel. After being collected from the vessel walls, the soot was dried in a stove at 120 °C for 24 h. In order to produce homogeneous suspensions, the soot particles were dispersed in *n*-hexane using an ultrasonic bath. The addition of the soot particles to the ceramic paper was carried out adding the suspension dropwise until complete impregnation, and then drying at room temperature.

The catalytic activity of the ceramic papers for the soot combustion was studied by temperature-programmed oxidation (TPO). For this purpose, the structured samples + soot were heated at 5 °C/min from room temperature up to 600 °C in O_2 (18%) + NO (0.1%) diluted in He (total flow 20 ml/min) in a flow equipment designed for this purpose. Identical experiments without NO in the feed were also carried out. The exhaust gases were analyzed with a Shimadzu GC-2014 chromatograph (with TCD detector). The diesel soot was homogeneously impregnated in ceramic paper discs 2 cm in diameter prior to the TPO experiment using a suspension of 600 ppm of diesel soot in *n*-hexane.

2.2.4.2. Experiments with soot collected from the exhaust pipe of a diesel engine. In order to collect real soot particles and to evaluate the mechanical resistance of the catalytic papers, some of them were introduced into a metallic housing and exposed to the exhaust of a Corsa 1.7 vehicle. After 30 min of exposure, samples of the catalytic paper impregnated with soot particles were taken, and TPO experiments were conducted at laboratory conditions.

2.3. Tensile strength

The tensile strength and stiffness of the ceramic papers were determined in an INSTRON 3344 universal tester, equipped with a load cell of 10 N, using the standard TAPPI T 576 pm-07 method to calculate the tensile properties of tissue papers. Ceramic paper sheets of about 0.002 m in thickness were cut as rectangles of 0.05 m in width and 0.07 m in length leaving a free length between grips of 0.05 m.

2.4. Permeation

To determine the permeation of the ceramic papers, a specific system was designed and constructed for this purpose (schematized in Fig. 2). It contained a cylindrical stainless steel piece inside which the ceramic paper discs (up to a maximum of 14) were piled up onto a wire mesh welded to one of the ends of the cylindrical container. Its respective flange and bolts created the closure of the reactor and a thermoplastic polymer sealed the joint.

Permeability coefficients, Ks, were calculated according to Darcy's Law:

Table 1
Composition of the catalytic ceramic papers.

Name[a,b]	CeO_2 content wt.%[c]	Atomic Ce content, wt%[c]	Atomic Co content, wt.%[d]	Co/(Co + Ce) (% mol)
10Ce-600	10	8.1	–	–
10Ce–Ce-600	41.7	33.8	–	–
10Ce–Co-600	10	8.1	9.6	32.1
10Ce–Ce–Co-600	43.1	34.9	8.9	24.9
10Ce–Co-900	10	8.1	9.6	32.1
10Ce–Ce–Co-900	43.1	34.9	8.9	24.9
20Ce-600	20	16.3	–	–
20Ce–Ce-600	35.3	28.6	–	–
20Ce–Co-600	20	16.3	6.0	26.8
20Ce–Ce–Co-600	34.8	28.2	7.8	27.6
20Ce–Co-900	20	28.6	6.0	26.8
20Ce–Ce–Co-900	34.8	28.2	7.8	27.6

[a] The number at the beginning indicates the wt.% of CeO_2 colloidal suspension used in the preparation, whereas the number at the end indicates the calcination temperature, in °C.
[b] Symbols between hyphens indicate the incorporation of either cobalt and/or cerium nitrates by impregnation over the calcined ceramic paper containing Ce Nyacol as a binder.
[c] The amount of cerium incorporated by impregnation was determined as the weight differences between those of calcined ceramic papers and the corresponding to ceramic paper after being impregnated with the $Ce(NO_3)_3$ and after calcination. The total amount of cerium loaded to the ceramic papers is reported in these columns, referred to the amount of ceramic fiber. It resulted from the addition of Ce incorporated as $Ce(NO_3)_3$ and Ce coming from the Nyacol colloidal suspension.
[d] The amount of cobalt incorporated by impregnation was determined as the weight differences between those of calcined ceramic papers and the corresponding of ceramic paper after being impregnated with $Co(NO_3)_2$ and after calcination. It is referred to the amount of ceramic fibers.

$$\frac{Q}{A} = \frac{K_S}{\eta}\frac{\Delta P}{L} \quad (1)$$

where Q is the measured air flow (ml/s), K_S the permeability coefficients (mm^2), A flow area (243 mm^2), ΔP pressure drop through the bed (bar), η viscosity of air at room temperature and pressure (bar s) and L the bed height (20 mm).

Q/A vs $\Delta P/L$ curves were obtained by changing the inlet air pressure and measuring the permeated air flow; the permeability coefficient (K_S) was obtained after the linear fitting from the slope.

3. Results and discussion

3.1. X-ray diffraction

Fig. 3A and B shows the XRD patterns of the different papers prepared. Although papers were calcined at 600 °C, no signals belonging to either Al_2O_3 or SiO_2 are observed, indicating the low cristallinity of these ceramic fibers. Signals observed for 10Ce-600 (at $2\theta = 28.6°$, 33.1°, 47.5°, 56.4° and 59.1°) correspond to the cubic fluorite-type structure of CeO_2 (JCPDS-ICDD 34-394). The same is observed for 10Ce–Ce-600. The addition of cobalt to these samples (10Ce–Co-600 and 10Ce–Ce–Co-600) provokes the appearance of peaks at $2\theta = 36.9°$, 65.3°, 31.3°, 59.4° and 44.8°, which correspond to the spinel structure of Co_3O_4 (JCPDS-ICDD 42-1467). Although both samples (10Ce–Co-600 and 10Ce–Ce–Co-600) contain approximately the same cobalt content, ca. 9 wt.%, the difference in the relative intensities between these signals should be ascribed to the different Ce content of these samples and to the fact that signals in Fig. 3 are values relative to the highest signal of CeO_2 (at 2θ 28.6°).

On the other hand, Liu et al. [11] and Wang et al. [15] studied the lattice parameters of $Co_xCe_{1-x}O_y$ samples by Rietveld refinement analysis and found that cobalt can be introduced into the CeO_2 lattice up to a content of 5 mol% (calculated as 100.Co/(Co + Ce). Therefore, at low Co loadings, a cobalt–cerium oxide solid solution is formed, while higher Co loadings cause the conglomeration of crystalline Co_3O_4. In our case, both 10Ce–Co-600 and 10Ce–Ce–Co-600 exceed this amount of cobalt, so that the solid solution is formed and excess Co is as Co_3O_4. As stated above, the relatively lower intensities of the Co_3O_4 peaks observed for 10Ce–Ce–Co-600 could be related to the higher amount of Ce in this sample (34.9 wt.%), in comparison to that of the 10Ce–Co-600 sample (8.1 wt.%). The former can accommodate more cobalt into its structure through the formation of the cobalt–cerium solid solution, so that the signals of Co_3O_4 in the corresponding XRD pattern are smaller. Besides, this low intensity of the Co_3O_4 peaks could be ascribed to a high dispersion of the cobalt spinel over the Ce nanoparticles layer.

When calcined at 900 °C, the crystalline phases are the same as those observed for samples calcined at 600 °C, although crystallinity increases, as observed by the width at the half high of the XRD peaks.

For ceramic papers prepared using a higher amount of Ce colloidal suspension (20 wt.% as CeO_2), despite a slightly higher amount of Ce, the total Ce content of 10Ce–Ce–Co-600 and 20Ce–Ce–Co-600 is similar (28.2 wt.% and 34.9 wt.%, respectively). Considering this, no significant differences would be expected in the corresponding XRD diffractograms.

3.2. Laser Raman spectroscopy

The Raman spectrum of 10Ce-600 shows the characteristic peak of CeO_2 at 465 cm^{-1}. The addition of cerium from the corresponding nitrate (10Ce–Ce-600) did not modify the Raman spectrum (Fig. 4). After the addition of cobalt (10Ce–Co-600 and 10Ce–Ce–Co-600 samples), besides the CeO_2 signal, the corresponding peaks of Co_3O_4 at 193, 482, 524, 612 and 688 cm^{-1} [16] were observed, in agreement with XRD results. Nevertheless, the intensity of the CeO_2 peak for 10Ce–Co-600 was lower. This can be ascribed to the deformation of the cubic fluorite structure of CeO_2 due to the presence of cobalt ions of lower valence than Ce^{+4}, thus decreasing the intensity of the 465 cm^{-1} peak [11]. As the cerium content of 10Ce–Co-600 is significantly lower than that of 10Ce–Ce–Co-600 and the cobalt content is almost the same (Table 1), the amount of cobalt that can be introduced into the CeO_2 fluorite structure is the same for both samples, "freer" CeO_2 remaining in the 10Ce–Ce–Co-600 sample, which correspondingly exhibits a more intense signal at 465 cm^{-1}.

The calcination at 900 °C does not modify the species observed by Raman. It is important to remark the absence of the 753 cm^{-1} signal, associated with the cobalt–aluminum spinel ($CoAl_2O_4$), which would indicate that the calcination up to 900 °C does not cause the interaction between cobalt species and the Al_2O_3 fibers.

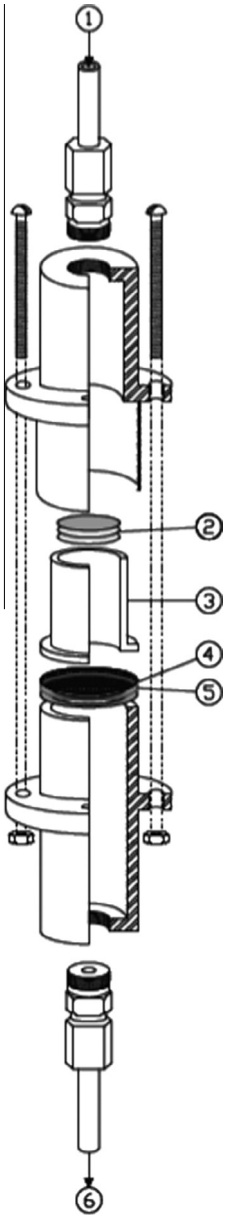

Fig. 2. Permeation reactor scheme. (1) Air inlet, (2) ceramic paper discs, (3) cylindrical reservoir, (4) wire mesh, (5) thermoplastic polymer seal and (6) air outlet.

In this sense, the CeO_2 nanoparticles added as binder would prevent this interaction.

Fig. 4 shows only the Raman spectra of ceramic papers prepared using 10 wt.% of CeO_2 Nyacol because no significant differences were observed in the samples containing 10 or 20 wt.% of CeO_2.

3.3. Scanning Electron Microscopy and Energy Dispersive X-ray Spectroscopy

Fig. 5 shows the morphology of ceramic papers containing only the Ce binder, i.e. before the impregnation of active ingredients, both before and after calcination. For sample 10Ce-600, an open mat made up of ceramic fibers can be observed in the general view picture. A close detail of a fiber shows how the Ce binder covers it completely and the corresponding magnification of the coverage shows that the CeO_2 nanoparticles are, in average, ca. 60 nm in diameter. The bottom part of Fig. 5 shows micrographs of the corresponding papers containing 20 wt.% CeO_2, where the first picture shows a fibrous mat of both ceramic and cellulosic fibers. These cellulosic fibers observed in the ceramic paper before calcinations (20Ce) contribute to the formation of the mat and favor the retention of particles during the papermaking process. A closer view shows the ribbon shape of cellulosic fibers, of about 6 μm in width and 3 mm in length (this latter value determined using an optical microscope [17]). It can also be seen that CeO_2 nanoparticles completely cover the ceramic fibers and also form patches over this monolayer. Moreover, these nanoparticles accumulate on fiber crossings due to tensoactive forces, thus joining them [18]. After the calcination of this ceramic paper (20Ce-600), the fiber appears covered by a layer of nanoparticles, as in the case of 10Ce-600, but for 20Ce-600, a higher amount of CeO_2 clusters (binder) can be observed. It is important to remark that the open structure obtained observed in the SEM micrographs after calcination of the ceramic papers is desirable for diesel soot filtering applications since a low drop pressure is an important variable to consider for practical purposes (diesel filter design). In addition, the porosity of the paper structure can be optimized by changing preparation procedures in order to improve the filtration efficiency. However, this point is beyond the scope of this work.

The idea behind incorporating either 10 or 20 wt.% CeO_2 from the Nyacol suspension was to study the effect of the binder content on both the morphology of ceramic papers and their strength and flexibility. SEM images indicated that the 10 wt.% CeO_2 Nyacol addition was enough to completely cover the ceramic fibers.

After the catalytic ingredients incorporation, a notable change in the morphology of ceramic papers was observed (Fig. 6). For 20Ce–Ce-600, besides CeO_2 patches formed by the binder, CeO_2 aggregates (clusters) appear distributed all along the ceramic paper structure. The size of these CeO_2 clusters varies between ca. 5 and 30 μm. When cobalt is also added (20Ce–Ce–Co-600), a higher amount of material (as CeO_2 and Co_3O_4) crystallizes between the ceramic fibers.

A closer view of 20Ce–Ce–Co-600 shows the ceramic fibers completely covered with CeO_2 nanoparticles, and over these, patches of oxides (CeO_2 and Co_3O_4) of about 1 μm in thickness. It was difficult to distinguish between CeO_2 and Co_3O_4 particles both by SEM and by EDX. The latter technique allowed determining that CeO_2 and Co_3O_4 resulted nonhomogeneously distributed.

The calcination at 900 °C results in a more open structure. Besides, the comparison between 20Ce–Co-600 and 20Ce–Co-900 shows that the crystal size of oxides in patch increases from ca. 60 nm to 100–150 nm when the calcination temperature increases from 600 to 900 °C. According to EDX results, more rounded-edge particles correspond to Co_3O_4, which preferentially sinters when calcination temperature increases, probably covering CeO_2 patches. This could diminish the exposed area of cobalt, probably affecting the activity of the catalytic ceramic paper.

3.4. Catalytic evaluation

3.4.1. Catalytic activity

Tables 2 and 3 summarize the tests of diesel soot combustion experiments using the different catalytic ceramic papers. Table 2 shows the results for papers calcined at 600 °C and Table 3 shows those of papers calcined at 900 °C, i.e. the temperatures at which 10% (T_{10}), 50% (T_{50}) and 90% (T_{90}) of soot are burned either in the presence of diluted O_2 or NO + O_2.

Ce nanoparticles confer to the ceramic paper a moderate activity towards soot combustion, since T_{50} is about 440 °C when feeding NO + O_2. The addition of Ce from $Ce(NO_3)_3$ to 10Ce-600 decreases the temperature necessary to achieve 50 and 90% soot conversion both under O_2 and NO + O_2 streams (Table 2). According to the preparation results (Table 1) and SEM micrographs (Figs. 5 and

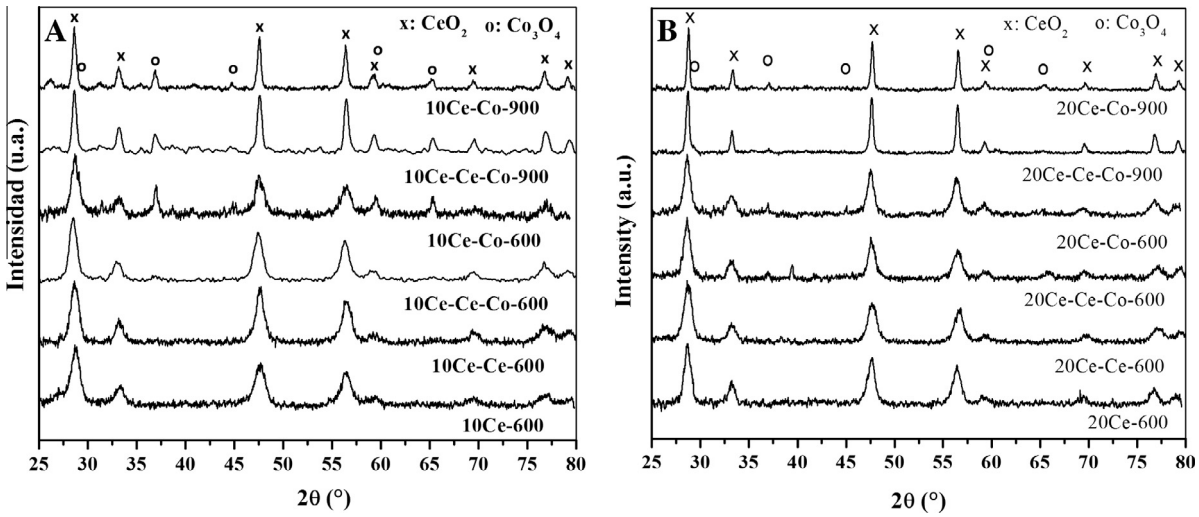

Fig. 3. XRD diffraction patterns of papers with CeO_2 colloidal used as binder. (a) 10 wt.% and (b) 20 wt.%.

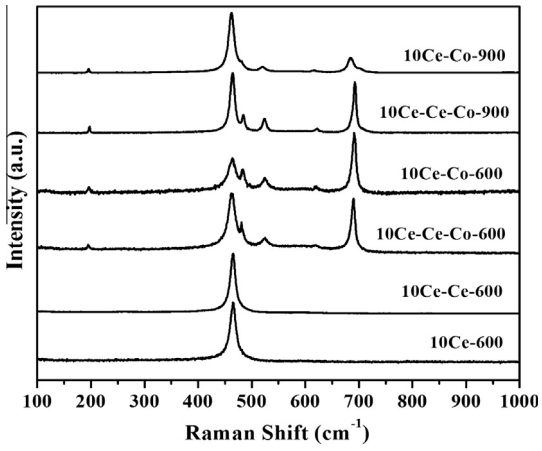

Fig. 4. Raman spectra of ceramic papers prepared with 10% of CeO_2 colloidal as binder.

6), CeO_2 Nyacol covers fibers and accumulates on them as patches whereas after calcination, the addition of Ce from its corresponding nitrate forms oxidic clusters.

The addition of Co provokes a notable increase in the catalytic activity, both under NO + O_2 and under O_2 diluted flows. Especially for 10Ce–Ce–Co-600 when feeding NO + O_2, T_{50} was 376 °C and T_{90} was 421 °C. Considering that the temperature of diesel vehicles exhaust varies between 350 and 450 °C, 10Ce–Ce–Co-600 appears as a good catalyst for practical purposes (diesel filter). For catalytic ceramic papers only impregnated with cobalt, the tendency is the same. Comparing 10Ce–Ce–Co-600 and 10Ce–Co-600, the former is more active towards soot combustion for the NO + O_2 feed, even though it has a slightly lower cobalt content. This could be related to its high Ce content, since CeO_2 is well known as an oxygen storage component and it is evident when NO + O_2 is fed to the reactor, due to the higher oxidation power of NO_2 in comparison with O_2. These results agree with those of previous studies, in which we found that CeO_2 would act as oxidation catalyst promoting the NO_2 formation and the consequent formation of NOx adsorbed species from the NO + O_2 stream [19].

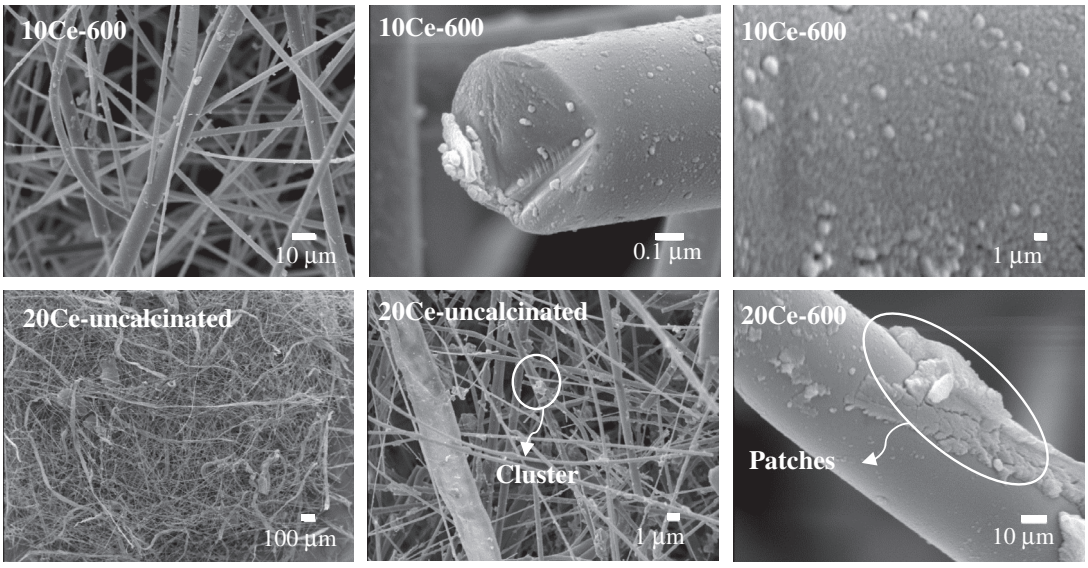

Fig. 5. SEM Microscopy. Morphology of papers with 10 and 20 wt.% of CeO_2 as binder, both calcined and uncalcined.

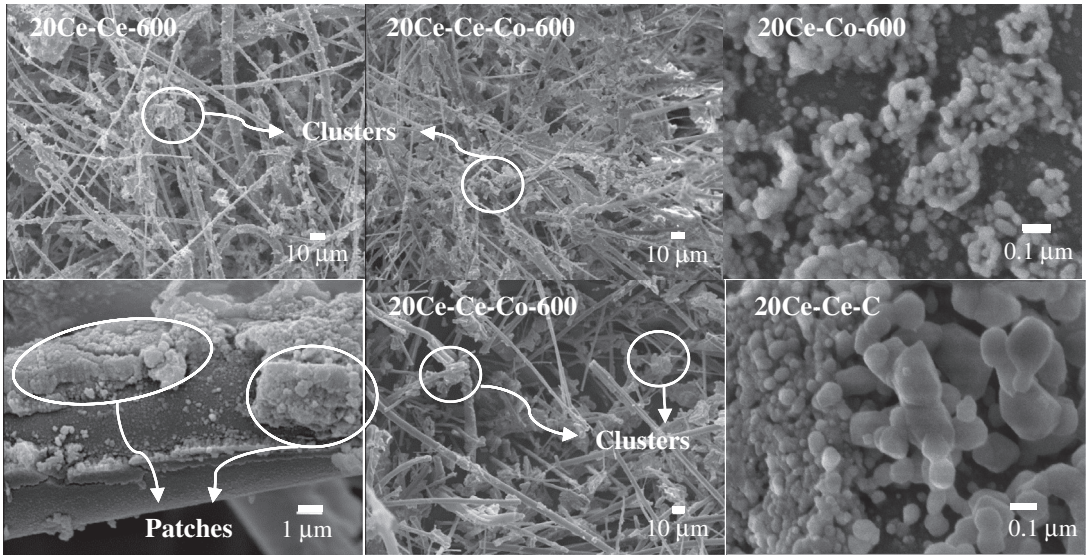

Fig. 6. Effect of both the addition of the catalytic ingredients and the calcination temperature on the morphology of ceramic papers.

Table 2
Summary of diesel soot TPO results using catalytic ceramic papers with 10% and 20% CeO_2 (Nyacol) calcined at 600 °C.

Ceramic papers	NO + O_2			O_2		
	T_{10} (°C)	T_{50} (°C)	T_{90} (°C)	T_{10} (°C)	T_{50} (°C)	T_{90} (°C)
10Ce-600	334	444	491	427	517	560
10Ce–Ce-600	303	422	462	391	483	530
10Ce–Co-600	303	396	442	334	459	504
10Ce–Ce–Co-600	303	376	421	380	466	517
20Ce-600	319	433	485	437	519	560
20Ce–Ce-60	335	424	467	380	479	529
20Ce–Co-600	299	395	454	385	491	542
20Ce–Ce–Co-600	295	391	434	356	456	509

Table 3
Thermal deactivation experiments using catalytic ceramic papers with 10% and 20% CeO_2 (Nyacol) calcined at 900 °C.

Ceramic papers	NO + O_2			O_2		
	T_{10} (°C)	T_{50} (°C)	T_{90} (°C)	T_{10} (°C)	T_{50} (°C)	T_{90} (°C)
10Ce–Ce–Co-900	334	422	488	417	526	571
10Ce–Co-900	365	470	529	420	521	570
20Ce–Ce–Co-900	345	438	495	438	513	569
20Ce–Co-900	371	488	540	388	523	562

When only O_2 is present, the role of CeO_2 as oxygen storage element is not significant, which is evidenced in the activity of 10Ce–Ce–Co-600 and 10Ce–Co-600 when feeding only diluted O_2.

No significant differences are found between papers containing either 10 or 20 wt.% of CeO_2 nanoparticles; this suggests that the content of Ce–Co clusters would enhance the catalytic activity whereas the relative amount of CeO_2 patches would not.

3.4.2. Catalysts deactivation

Since the best catalysts were those that contained both CeO_2 clusters and Co_3O_4, the thermal stability of these systems was studied. For this purpose, catalytic ceramic papers were calcined at 900 °C for 2 h; then, their activity towards soot combustion was evaluated and compared with those of papers calcined at 600 °C. Fig. 7 shows the effect of the calcination temperature on papers prepared using 10 wt.% CeO_2 Nyacol. As expected, all TPO curves shift to higher temperatures when the calcination temperature increases.

When feeding both NO and O_2, there appear differences between the catalytic behavior of 10Ce–Co-600 and 10Ce–Ce–Co-600 (Fig. 7A and B). The presence of Ce clusters (generated by $Ce(NO_3)_3$ addition) led to a lower deactivation of the catalyst. On the contrary, under O_2 stream (Fig. 7C and D), the presence of Ce clusters does not prevent the thermal catalysts deactivation. As stated above, the role of CeO_2 as oxygen storage element is more evidenced when feeding NO + O_2.

In order to gain further insight into the deactivation process, some other points should be addressed. First, a decrease in the external surface area occurs due to oxides sintering on patches, as observed by SEM (Fig. 6). In addition, clusters are broken, where part of this material is lost, and fibers become brittle. And probably, the incipient formation of CoO (not active as oxidation catalyst), not observed by XRD, should be considered, according to Ivas et al. [20]. The formation of the inactive $CoAl_2O_4$ spinel (although not seen by either XRD or Raman techniques) should not be discarded.

Besides, an increase in the cobalt spinel crystallite size is observed by XRD and these Co_3O_4 conglomerates would be less active. This would agree with results reported by Liu et al. [11], who found better activities towards soot combustion when depositing cobalt oxide on nanometric CeO_2 particles, whereas high Co loading induced a Co_3O_4 conglomeration that led to a lower activity for soot combustion. Therefore, the cobalt deposition on the CeO_2 nanoparticles that cover the ceramic fibers would enhance cobalt dispersion forming catalytic species with higher activity towards soot combustion than the cobalt conglomerates deposited on CeO_2 clusters [21]. The increment in the crystallite size of cobalt species would affect less when Ce clusters are present under NO + O_2 (Fig. 7A and B) due to the higher oxidant power of NO + O_2 in comparison with that of O_2.

For catalysts prepared with 20 wt.% CeO_2 Nyacol the deactivation process is similar to that of samples prepared with 10 wt.% CeO_2 Nyacol both under O_2 or NO + O_2 streams.

In order to better clarify the deactivation of catalytic active species and catalytic ceramic papers, Fig. 8 schematizes the species that form the different catalytic ceramic papers. It can be observed

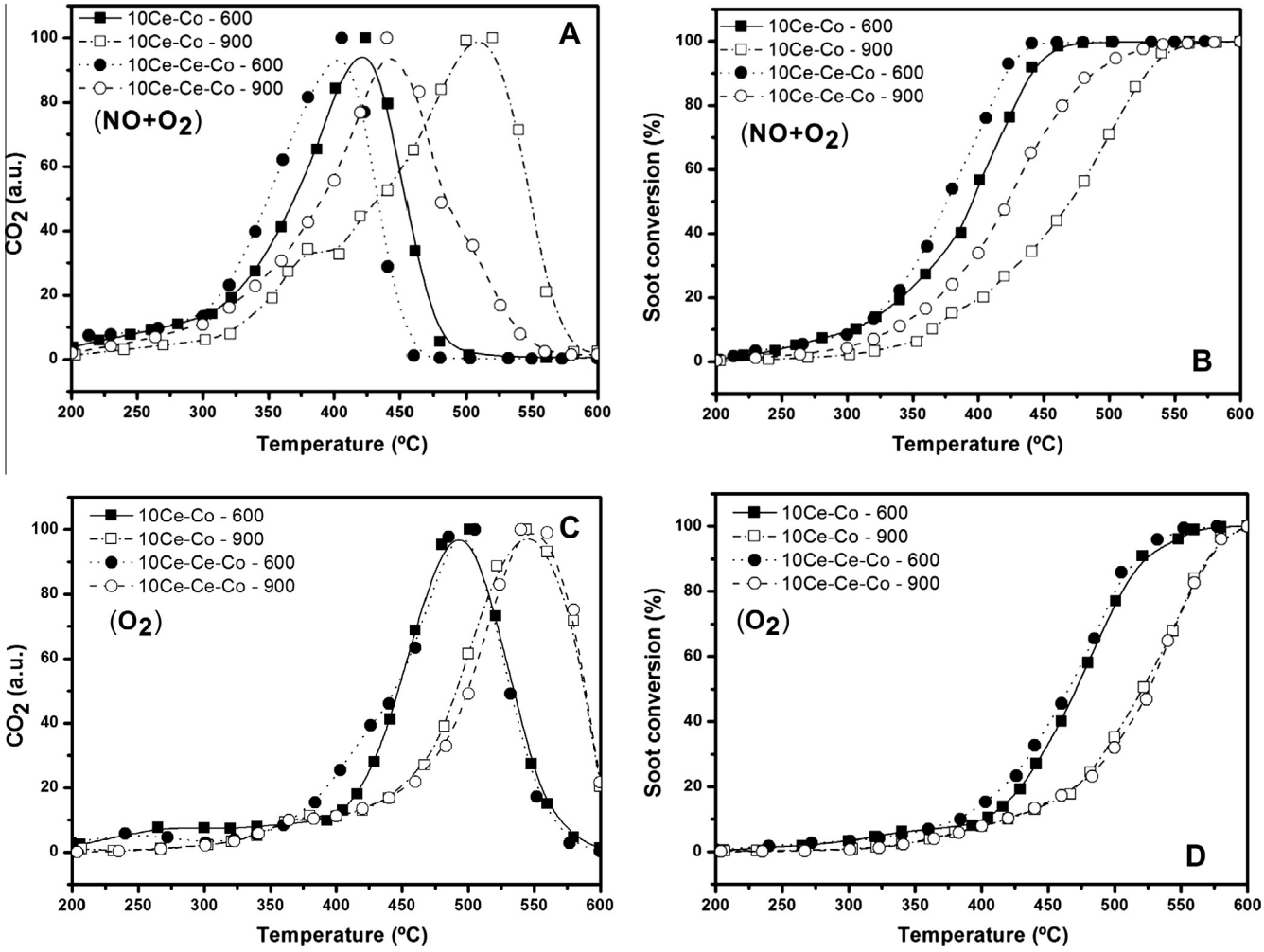

Fig. 7. Catalytic activity of papers impregnated with 10% CeO_2 as binder both calcined at 600 °C and 900 °C. (A) Production of CO_2 as a function of temperature under NO + O_2 stream (He balance) and (B) Soot Conversion (%). (C) Production of CO_2 as a function of temperature under O_2 stream (He balance) and (D) Soot Conversion (%). Feed composition: NO (0 or 0.1%, as indicated), O_2 (18%) (He balance).

how cerium nanoparticles completely cover ceramic fibers, in which cerium excess forms CeO_2 patches, whereas the addition of both Ce and Co nitrates that produce the corresponding clusters in the intersections among fibers can also be observed. The effect of the calcination temperature is evident through the more rounded edges of clusters and patches.

In addition to all this, after calcination at 900 °C, papers resulted fragile, very difficult-to-handle, as Fig. 9 shows. It is important to remark that although deactivation studies are necessary, the diesel soot filter is not expected to operate at these high temperatures.

3.5. Mechanical properties

Fig. 9 shows the curves obtained with the INSTRON apparatus, where Tensile Load is plotted against Elongation. The maxima of the curves, i.e. breaking loads (BL, N), and the slopes at the straight parts of the curves ($\Delta F/\Delta L$, N m^{-1}) allowed calculating the Tensile Indexes (TI, N m g^{-1}) and the Elastic Modules (MPa), as indicated below (Eqs. (2) and (3)).

$$TI = \frac{BL}{G.W} \tag{2}$$

$$EM = \frac{10^{-6}.\Delta F/S}{\Delta L/L} \tag{3}$$

where G is the grammage (weight per surface unit, g m^{-2}), W is the paper strip width (0.05 m), S (m^2) is paper section calculated as probe width (0.05 m) multiplied by paper thickness and L (0.05 m), which is the distance between the testing grips at the beginning of the experiment (before paper probe elongation).

It should be stressed that a high tensile index and a low elastic modulus (high elasticity) are the desired characteristics of a ceramic paper.

Fig. 9 shows the complete curves to point out that during these tests, failure does not occur as a "clean rupture". Instead, paper tearing occurs, individual ceramic fibers break and many of them are pulled out during the rupture. For this reason, each experiment was carried out eight times at least (except for the paper calcined at 900 °C due to its fragility) and Fig. 9 shows the most representative curves. Nevertheless, the values reported in Table 4 consider all the results obtained, so that average values are listed with their corresponding confidence interval.

Similar tensile index and elastic modulus values are observed for both 10Ce-600 and 20Ce-600, which implies that the increase from 10 to 20 wt.% CeO_2 Nyacol did not enhance the mechanical properties of ceramic papers (Fig. 9, Table 4). As observed by SEM (Fig. 5), higher amounts of colloidal Ce are deposited as oxidic clusters among ceramic fibers. However, as observed in the mechanical tests, these clusters confer neither more resistance nor more elasticity to ceramic papers.

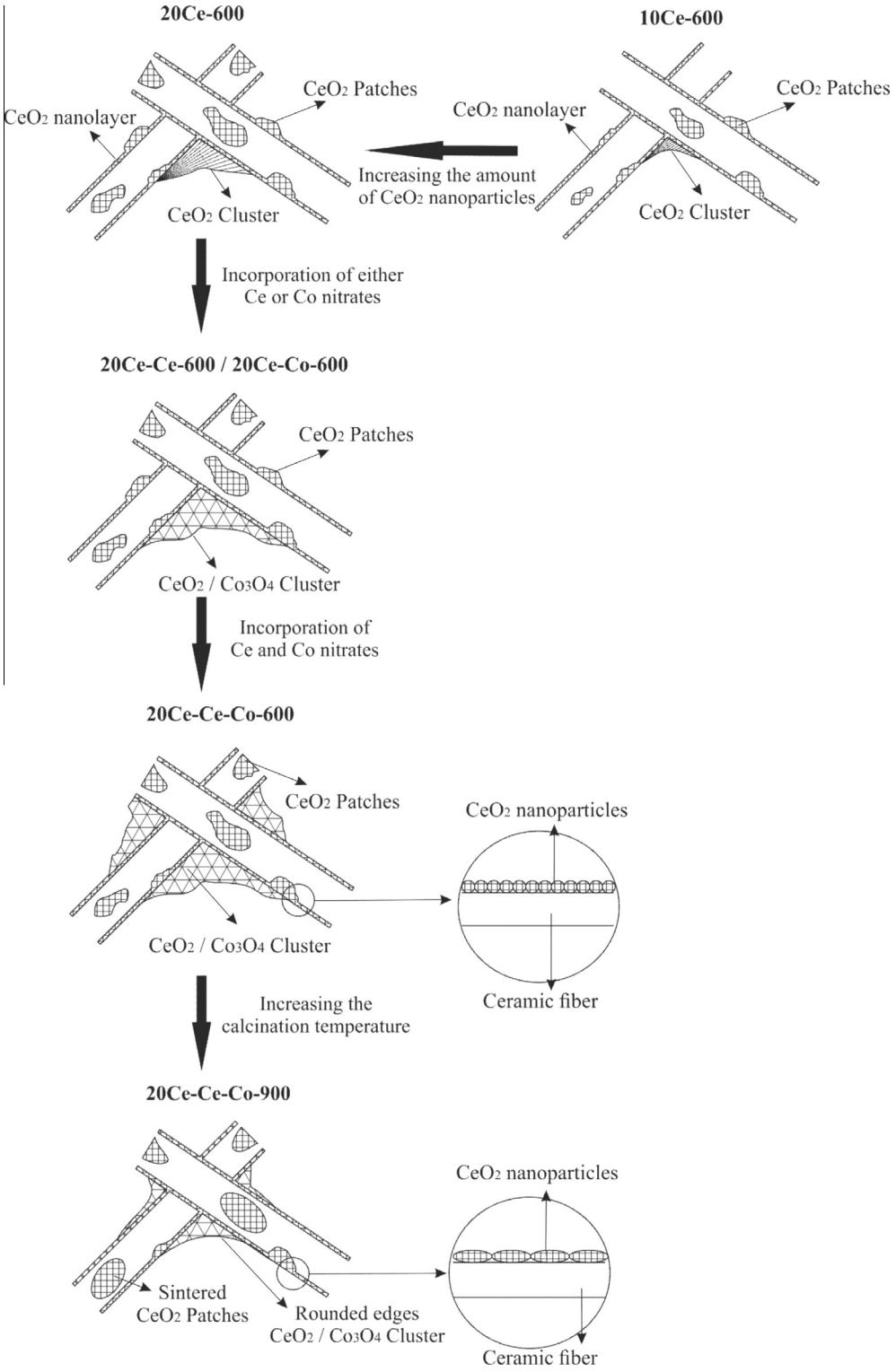

Fig. 8. Scheme of catalytic ceramic papers morphology.

The addition of both Ce and Co from their corresponding nitrates makes ceramic papers calcined at 600 °C (20Ce–Ce–Co-600) more resistant but less elastic. In fact, the tensile index value increases from 0.15 to 0.34 N m g^{-1} whereas the elastic modulus increases from 3.15 to 14.74 MPa. After calcination at 900 °C, the structure of the ceramic paper results very fragile, and correspondingly the tensile index value decreases and the elastic modulus value increases, in detriment of mechanical properties. Nevertheless, as stated above, it is not expected that ceramic filters should operate at this high temperature.

Results show that ceramic papers have lower tensile index values but similar elastic modulus if compared with a commercial tissue paper (see Table 4). Nevertheless, as Fig. 9 shows, the photographs of rolled papers highlight the ceramic papers flexibility. The picture shows a rolled piece of 10Ce-600, which is yellow whereas cobalt-containing papers are black.

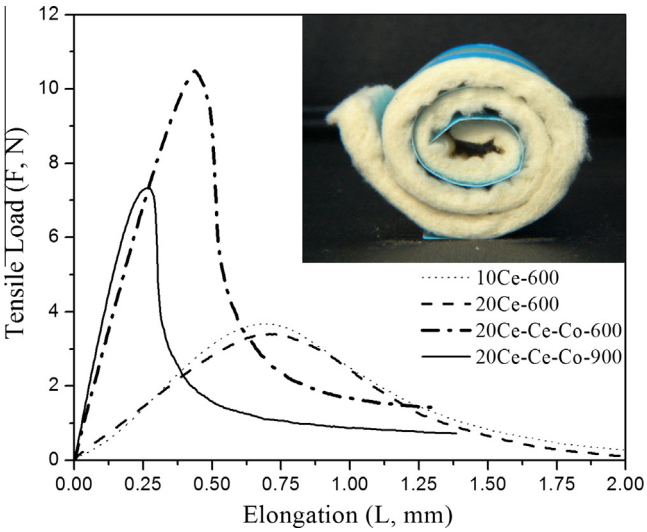

Fig. 9. Mechanical behavior: curves obtained for ceramic papers (a) the tensile index (TI) was determined from the corresponding breaking load value, indicated by the square, and the specific elastic modulus (EM) was calculated from the slope of the elastic portion of the curve (b) and (c) are pictures of rolled pieces of catalytic ceramic papers, in which the paper thickness is ca. 2 mm.

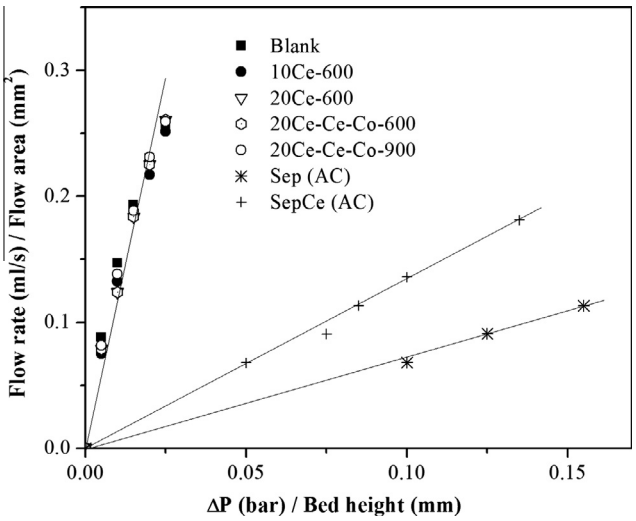

Fig. 10. Paper permeation curves: air flow permeated as a function of the difference of applied pressure. Comparison whit results reported in the literature for sepiolite as a filter of soot particles.

3.6. Permeation and soot filtration properties

Fig. 10 shows the Q/A vs $\Delta P/L$ curves obtained for the different tested ceramic papers and the curve corresponding to the empty reactor which only contains a bottom metallic mesh. No differences between permeability of ceramic papers were observed; as expected, the open structure of these materials exhibit high permeability, similar to that obtained for the single metallic mesh used to contain ceramic papers. For all tested papers, an average K_S value of 2.0 10^{-6} mm^2 could be calculated. The high permeability of ceramic papers, which causes very low pressure drops, is a desirable property if the potential application of these structures as diesel soot filters is considered.

In order to compare the permeability of ceramic papers with that of more compact and commonly used structures, permeation curves for porous sepiolite ceramic monoliths were included in Fig. 10 [22]. As can be easily seen, ceramic papers are significantly more permeable, K_S values being about 10 times higher than those of sepiolite monoliths. Considering that these ceramic papers could potentially be used as soot filters, a good particulate retention capacity would also be desirable. For this purpose, preliminary experiments in a testing bench were performed, in which ceramic papers were introduced in a specially designed metal housing. Fig. 11 shows images of the open housing, with a piece of ceramic paper on top. The complete structure consists of two identical parts as shown in Fig. 11A, connected through flanges and bolts, where the ceramic paper disc is located between metallic meshes. This structure has couplings to connect with the diesel engine exhaust. For these previous tests, an engine of a Corsa 1.7 diesel vehicle was used. Fig. 11B and C shows how soot is retained in the whole filter and especially on the face exposed to the exhaust gases. It is also seen that the filter developed based on ceramic papers resisted the real conditions existing in the exhaust pipe (very high gas flows, in the order of 2 m^3 min^{-1}). It should be remarked that in this experiment the catalytic paper was tested only as a filter, because it was located far from the engine exhaust and, consequently, where temperature is not enough for the filter self-regeneration.

Since the temperature in the pipe where the filter is placed was not enough to catalytically burn the soot, the catalytic ceramic paper (10Ce–Ce–Co-600) with soot extracted from the metallic housing was cut into pieces and evaluated in laboratory. Therefore, this test was performed using a real contact between soot and the catalyst. As Fig. 12A shows, the TPO profile indicates the presence of two peaks, with maxima at 330 °C and 513 °C, where the peak at higher temperature exhibits a shoulder at lower temperatures. In order to identify the peak corresponding to the catalytic combustion of soot, another experiment was carried out. Fig. 12B shows the TPO profile of a piece of the same catalytic ceramic paper extracted from the testing bench as shown in Fig. 12A, but milled in a mortar so as to achieve tight contact between the carbonaceous material and the catalyst incorporated to the ceramic paper. This latter case indicates that soot in tight contact with the Ce–Co-containing ceramic paper burns with a maximum at 428 °C. The corresponding deconvolution of Fig. 12A exhibits all these three peaks: the one appearing at 330 °C corresponding to the catalytic combustion of unburned hydrocarbons adsorbed on soot, the one with a maximum at 450 °C corresponding to the catalytic burning of soot in tight contact with the catalyst, and the one with a maximum at 513 °C corresponding to the catalytic burning of soot in

Table 4
Mechanical properties of catalytic ceramic papers.

Ceramic paper	Tensile index (N m g^{-1})	Confidence interval[a] (N m g^{-1})	Elastic module (MPa)	Confidence interval[a] (MPa)
10Ce-600	0.15	0.02	3.36	0.38
20Ce-600	0.15	0.02	3.15	0.47
20Ce–Ce–Co-600	0.34	0.03	14.74	1.91
20Ce–Ce–Co-900	0.20	0.15	22.13	4.82
Commercial paper 1	3.81	0.22	6.65	0.22
Commercial paper 2	10.03	0.72	11.79	0.57

[a] Calculated using the Dixońs Q test.

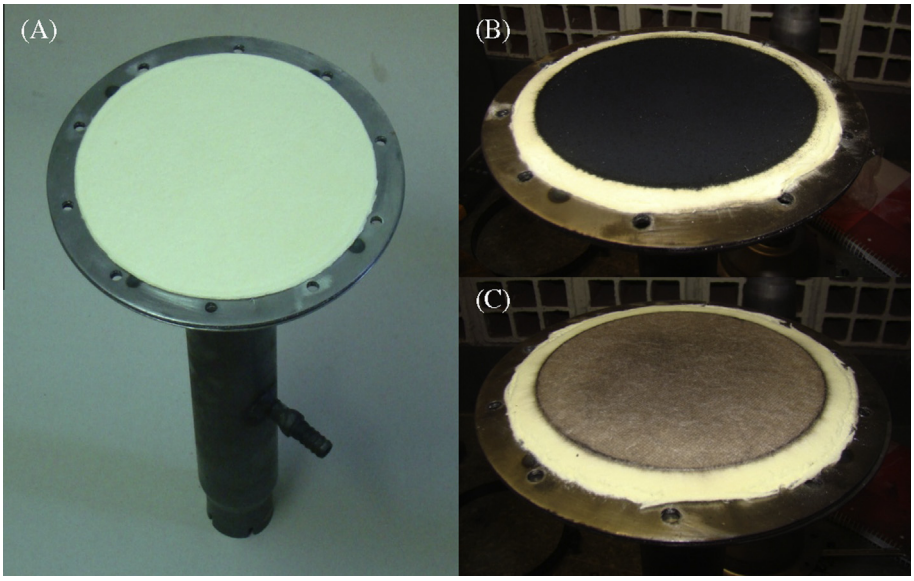

Fig. 11. Ceramic papers disposal for their evaluation in a test bench. Part of the designed metallic housing with a ceramic paper disc (a) before, (b) after the test, exposed face to the gas flow and (c) after the test, face opposite to the flow. The picture shows an experiment performed with a ceramic paper disc without cobalt so as to visualize the different colors before and after soot retention.

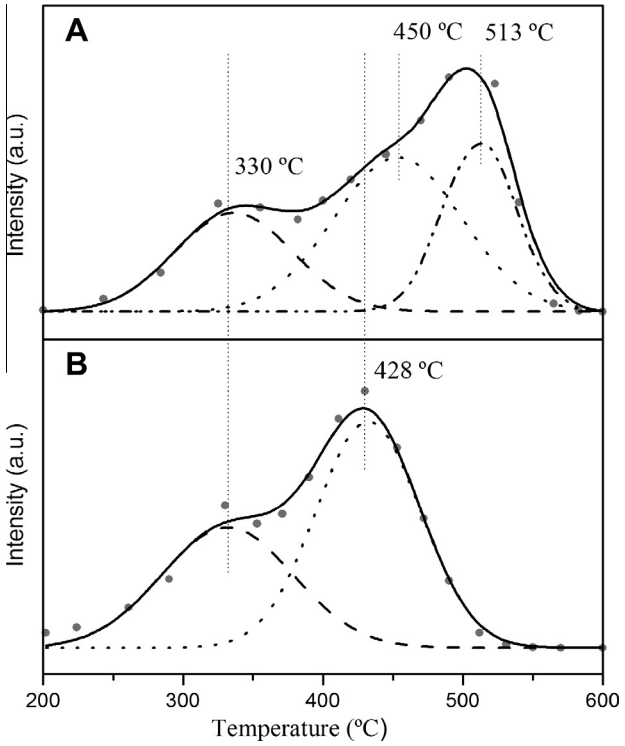

Fig. 12. TPO experiment with a portion of the ceramic paper disc (10Ce–Ce–Co-600) after its evaluation in the testing bench (a) and the same as the former, but milled, so as to achieve tight contact between the soot and the catalyst (b). Feed composition: NO (0.1%), O_2 (18%) (He balance).

loose contact with the catalyst. Considering that the catalytic combustion of soot implies two solids and one gaseous reagent, the lower temperature (428 °C) observed for the milled ceramic disc would be due to a higher number of catalytic particles in contact with the carbonaceous material.

Although further experiments should be carried out, these results are encouraging to continue exploring this promising system.

4. Conclusions

- The papermaking technique allowed us to obtain catalytic ceramic papers which were flexible, easy to handle and resistant to the exhaust gases from a diesel engine under real conditions.
- The CeO_2 nanoparticles that were added as binder elements completely covered the ceramic fibers, and also formed patches on this coverage. As the amount of CeO_2 nanoparticles increased, a greater number of bigger CeO_2 patches was formed.
- The addition of Ce and/or Co by impregnating the ceramic papers with solutions of the corresponding nitrates brought about the appearance of oxidic clusters.
- The catalytic activity of the ceramic papers was mainly related to the presence of oxidic clusters while the addition of CeO_2 nanoparticles between 10 and 20 wt.% did not contribute to the catalytic activity significantly. The TPO experiments indicated that in the presence of NO + O_2, the temperature at which the maximum soot combustion rate occurred was approximately 400 °C for 10Ce–Ce–Co-600 and T_{50} = 376 °C.
- The presence of Ce clusters makes the catalytic ceramic papers deactivate less after a thermal treatment at 900 °C.
- Preliminary experiments in a test bench showed that ceramic papers adequately resisted the high diesel engine exhaust flows (2 m^3 min^{-1}). Besides, it was also found that the soot in tight contact with the catalytic ceramic papers of the filters catalytically burned with a maximum rate at 428 °C, thus encouraging us to go deeper into the study of these ceramic papers for their use in the making of diesel particle filters. At present, studies are being carried out to determine the retention efficiency of the particulate matter and to optimize to porous structure of the papers.

Acknowledgments

The authors wish to acknowledge the financial support received from ANPCyT, CONICET, SECTEI Santa Fe and UNL. Thanks are also given to Elsa Grimaldi for the English language editing.

References

[1] M.V. Twigg, Catalytic control of emissions from cars, Catal. Today 163 (2011) 33–41.
[2] D. Fino, Diesel emission control: catalytic filters for particulate removal, Sci. Technol. Adv. Mater. 8 (2007) 93–100.
[3] http://www.ceraclean.com/fr/download/PKW_LightVehicles_EU.pdf.
[4] M. Yu, D. Luss, V. Balakotaiah, Regeneration modes and peak temperatures in a diesel particulate filter, Chem. Eng. J. 232 (2013) 541–554.
[5] H. Ström, S. Sasic, B. Andersson, Design of automotive flow-through catalysts with optimized soot trapping capability, Chem. Eng. J. 165 (2010) 934–945.
[6] G. Walther, B. Klöden, T. Büttner, T. Weißgärber, B. Kieback, A. Böhm, D. Naumann, S. Saberi, L. Timberg, A new class of high temperature and corrosion resistant nickel-based open-cell foams, Adv. Eng. Mater. 10 (2008) 803–811.
[7] P.A. Kumar, M.D. Tanwar, S. Bensaid, N. Russo, D. Fino, Soot combustion improvement in diesel particulate filters catalyzed with ceria nanofibers, Chem. Eng. J. 207–208 (2012) 258–266.
[8] C.A. Neyertz, E.E. Miró, C.A. Querini, K/CeO_2 catalysts supported on cordierite monoliths: diesel soot combustion study, Chem. Eng. J. 181–182 (2012) 93–102.
[9] H. Koga, H. Ishihara, T. Kitaoka, A. Tomoda, R. Suzuki, H. Wariishi, NO_X reduction over paper-structured fiber composites impregnated with Pt/Al_2O_3 catalyst for exhaust gas purification, J. Mater. Sci. 45 (2010) 4151–4157.
[10] E.D. Banús, M.A. Ulla, M.V. Galván, M.A. Zanuttini, V.G. Milt, E.E. Miró, Catalytic ceramic paper for the combustion of diesel soot, Catal. Commun. 12 (2010) 46–49.
[11] J. Liu, Z. Zhao, J. Wang, C. Xu, A. Duan, G. Jiang, Q. Yang, The highly active catalysts of nanometric CeO_2-supported cobalt oxides for soot combustion, Appl. Catal. B: Environ. 84 (2008) 185–195.
[12] M. Dhakad, T. Mitshuhashi, S. Rayalu, Pradip Doggali, S. Bakardjiva, J. Subrt, D. Fino, H. Haneda, N. Labhsetwar, Co_3O_4–CeO_2 mixed oxide-based catalytic materials for diesel soot oxidation, Catal. Today 132 (2008) 188–193.
[13] P.G. Harrison, I.K. Ball, W. Daniell, P. Lukinskas, M. Céspedes, E.E. Miró, M.A. Ulla, Cobalt catalysts for the oxidation of diesel soot particulate, Chem. Eng. J. 95 (2003) 47–55.
[14] E.D. Banús, M.A. Ulla, E.E. Miró, V.G. Milt, Co, Ba, K/ZrO2 coated onto metallic foam (AISI 314) as a structured catalyst for soot combustion: Catalytic activity and stability, Appl. Catal. A: General 393 (2011) 9–16.
[15] J. Wang, M. Shen, J. Wang, J. Gao, J. Ma, S. Liu, CeO_2–CoO_x mixed oxides: structural characteristics and dynamic storage/release capacity, Catal. Today 175 (2011) 65–71.
[16] V.G. Milt, M.A. Ulla, E.E. Miró, NOx trapping and soot combustion on $BaCoO_{3-y}$ perovskite: LRS and FTIR characterization, Appl. Catal. B: Environ. 57 (2005) 13–21.
[17] J.P. Cecchini, R.M. Serra, M.A. Ulla, M.A. Zanuttini, V.G. Milt, Enhancing mechanical properties of ceramic papers loaded with zeolites using borate compounds as binders, Bioresources 8 (1) (2013) 313–326.
[18] J.M. Zamaro, M.A. Ulla, E.E. Miró, The effect of different slurry compositions and solvents upon the properties of ZSM5 washcoated cordierite honeycomb for the SCR of NOx with methane, Catal. Today 107–108 (2005) 86–93.
[19] V.G. Milt, C.A. Querini, E.E. Miró, M.A. Ulla, Abatement of diesel exhaust pollutants. NOx adsorption on Co, Ba, K/CeO_2 catalysts, J. Catal. 220 (2003) 424–432.
[20] T. Ivas, A.N. Grundy, E. Povoden-Karadeniz, L.J. Gauckler, Phase diagram of CeO_2–CoO for nano-sized powders, Calphad 36 (2012) 57–64.
[21] Z. Zhao, M.M. Yung, U.S. Ozkan, Effect of support on the preferential oxidation of CO over cobalt catalysts, Catal. Commun. 9 (6) (2008) 1465–1471.
[22] V.G. Milt, E.D. Banús, E.E. Miró, M. Yates, J.C. Martín, S.B. Rasmussen, P. Ávila, Structured catalysts containing Co, Ba and K supported on modified natural sepiolite for the abatement of diesel exhaust pollutants, Chem. Eng. J. 157 (2010) 530–538.